

THE PALOMAR ABELL CLUSTER OPTICAL SURVEY. I. PHOTOMETRIC REDSHIFTS FOR 431 ABELL CLUSTERS

R. R. GAL,¹ R. R. DE CARVALHO,² R. BRUNNER, S. C. ODEWAHN,³ AND S. G. DJORGOVSKI
Palomar Observatory, California Institute of Technology, Mail Stop 105-24, Pasadena, CA 91125

Received 2000 April 14; accepted 2000 May 5

ABSTRACT

This paper presents photometric redshifts for 431 Abell clusters imaged as part of the Palomar Abell Cluster Optical Survey, of which 236 are new redshifts. We have obtained moderately deep, three-band (Gunn *gri*) imaging for this sample at the Palomar Observatory 60 inch (1.5 m) telescope, as part of the photometric calibration of the Digitized Second Palomar Sky Survey. Our data acquisition, reduction, and photometric calibration techniques are described, and photometric accuracy and consistency are demonstrated. An empirical redshift estimator is presented, utilizing background-corrected median $g - r$ colors and mean g magnitudes for the ensemble of galaxies in each field. We present photometric redshift estimates for the clusters in our sample with an accuracy of $\sigma_z = 0.038$. These redshift estimates provide checks on single-galaxy cluster redshifts, as well as distance information for studies of the Butcher-Oemler effect, luminosity functions, mass-to-light ratios, and many other projects.

Key words: catalogs — galaxies: clusters: general — surveys

1. INTRODUCTION

Clusters of galaxies are the largest bound systems in the universe, providing useful constraints for theories of large-scale structure formation and evolution. They are the samples of choice for studying galaxy evolution in dense environments, with many tens or even hundreds of galaxies in a small, physically associated volume. Multicolor optical photometry of galaxy clusters is commonly used to study the Butcher-Oemler effect (Butcher & Oemler 1978), the morphology-density relation (Dressler 1980), and other correlations between overall cluster properties, galaxy properties, and redshift. Comparisons between optical and X-ray properties of galaxy clusters are also of considerable scientific interest. For instance, mass-to-light ratios of clusters are also useful for constraining cosmological parameters, including Ω , the mass density of the universe. Properly understood catalogs in the optical and X-ray can help us better understand the various selection effects present in both types of cluster samples.

To obtain the maximal scientific return from such studies, it is necessary to know the redshifts of the clusters. Unfortunately, the majority of known galaxy clusters do not have measured redshifts. Nearly 50 years have passed since the publication of Abell's (1958) optically selected cluster catalog, and only about one-third of the northern clusters have had spectroscopically measured redshifts, with many of these based on only one or two galaxies. Even at low redshift, obtaining accurate cluster redshifts requires a 4 m-class telescope with multiobject spectroscopic capability; performing a survey of hundreds or even thousands of clusters is prohibitively time consuming.

In recent years, there has been an increasing recognition that redshifts of individual objects or clusters can be estimated quite accurately from photometric data (for example,

Frei & Gunn 1994; Brunner et al. 1997). These estimators have traditionally relied on either empirical correlations between individual galaxy colors and spectroscopically measured redshifts (Connolly et al. 1995) or a template method wherein model spectra are created from evolutionary synthesis codes or spectroscopic data (Gwyn & Hartwick 1996). However, both techniques aim to measure the redshifts of single objects using many ($n \geq 4$) colors; increasing the number of colors results in more accurate redshifts over a larger redshift range. An extensive discussion and comparison of existing techniques can be found in Hogg et al. (1998). Unlike these methods, we are instead relying on only two filters (Gunn *g* and *r*) to derive photometric redshifts for an ensemble of objects (a galaxy cluster) over a relatively small redshift range ($0 < z < 0.3$). Earlier methods for estimating cluster redshifts have generally relied on the magnitude of the n th brightest galaxy (Abell 1958; Dalton et al. 1994).

Using a small (1 m class) telescope, equipped with a large-format CCD, one can obtain photometric data on a very large sample of clusters. Greater amounts of observing time are more readily scheduled on such telescopes, and the integration times required for imaging are much shorter than for spectroscopy to comparable depths on larger telescopes. In addition, many optical imaging surveys, such as the Digitized Second Palomar Sky Survey (DPOSS; Djorgovski et al. 1999) and the Sloan Digital Sky Survey (SDSS; Gunn & Weinberg 1995), provide photometric data that can be used for this purpose. For instance, Gal et al. (2000) presented a simple photometric estimator for galaxy clusters found in DPOSS, and the SDSS photometric system (Fukugita et al. 1996) was designed specifically to improve photometric redshift estimation.

The success of these estimators spurred us to utilize our data on Abell clusters to measure their redshifts photometrically. We have observed 468 Abell clusters at the Palomar 60 inch (1.5 m) telescope, using two different detectors, in the Gunn *gri* filters (Thuan & Gunn 1976; Wade et al. 1979). The primary purpose of these data is to provide precision photometric calibration for DPOSS. Nevertheless, this large, homogeneous data set is a valuable resource

¹ rrg@astro.caltech.edu.

² Observatório Nacional, Rua General José Cristino 77, 20921-400 São Cristóvão, Rio de Janeiro, RJ, Brazil.

³ Department of Physics and Astronomy, Arizona State University, Box 871504, Tempe, AZ 85287-1504.

in and of itself and is ideal for photometric redshift estimation.

In § 1 of this paper, we describe the telescope, CCD cameras, and data-taking strategy used during the course of this survey. Section 2 describes the observing program. Section 3 presents our data reduction procedure and the derivation of photometric calibration, using Gunn standards, which were imaged every night. We also demonstrate our photometric accuracy using data acquired on the same clusters on multiple nights and with different detectors. Section 4 presents the photometric redshift estimation technique and our estimated redshift errors, as well as a table of the measured redshifts. We conclude with a brief discussion of our results (§ 5).

2. DATA ACQUISITION AND ANALYSIS

2.1. Telescope and Detectors

All data described in this paper were obtained at the Palomar Observatory 60 inch (1.5 m) telescope. The telescope is an f/8.75 Ritchey-Chrétien design, with the CCD imaging cameras placed at Cassegrain focus. From the initial data through 1996 June and on rare occasions thereafter, we used CCD16, a SITe 1024², thinned, AR-coated array, with 24 μm pixels. The pixel scale is 0''.376 pixel⁻¹, providing a 6.4×6.4 field of view (FOV). CCD16 has a gain of $2.5 \text{ e}^- \text{ DN}^{-1}$ and a read noise of 8.2 e^- . Starting in July 1996, a new, larger detector was made available at the Palomar 60 inch telescope. This detector, CCD13, is an SITe 2048² thinned, AR-coated array, also with 24 μm pixels. The pixel scale at this detector is 0''.368 pixel⁻¹, providing a 12.56×12.56 FOV. CCD13 has a gain of $1.63 \text{ e}^- \text{ DN}^{-1}$ and a read noise of 6.3 e^- . In addition to the factor of 4 increase in area compared with CCD16, this detector also provides extremely good blue sensitivity ($\sim 55\%$ quantum efficiency at 4000 Å). All objects were observed in the Gunn *gri* filters.

2.2. Observations

The imaging targets are selected from the list of northern Abell clusters (Abell, Corwin, & Olowin 1989). Because the survey was designed to provide photometric calibration and star-galaxy separation data for DPOSS (Djorgovski et al. 1999), we attempted to observe at least two Abell clusters per DPOSS field (each field being ~ 36 deg²). Priority was given to the richest clusters closest to the plate centers; therefore, our sample is biased toward richer Abell clusters. Nevertheless, many plates have only one or two known clusters; in such cases, whatever clusters were available were observed. Approximately 50 clusters were observed twice, sometimes with both detectors. This allows us to check our photometric accuracy, as well as consistency between detectors.

Data were taken only on photometric nights with seeing better than 2''. The mean seeing for our data is $\sim 1''.5$; the best seeing is 0''.9. Integration times were fixed for each filter-CCD combination, regardless of sky brightness or seeing. The vast majority of nights allocated for this program were more than 75% dark. For CCD16, we integrated for 1200 s in *g*, and for 900 s each in *r* and *i*. When using CCD13, the integration times were shortened to 900 s in *g* and to 600 s each in *r* and *i*. These yielded limiting magnitudes of $m_{\text{lim,gri}} \sim 22$ for CCD13 observations, with limiting magnitudes for CCD16 observations ~ 0.5 mag

brighter. With the typical observational overhead, we usually observed between seven and 11 clusters in a single night.

For every night that was deemed photometric, we observed a set of Gunn standards. Between five and 12 observations of available Gunn standards were made each night, at a variety of air masses. Each star observed at each pointing was observed three times on a single frame by closing the shutter, offsetting the telescope, and reopening the shutter. This was done to increase the signal-to-noise ratio of our photometric measurements, as well as avoid excessive time loss due to the long (~ 180 s) readout time for CCD13. In addition to the standard stars, we also took nine bias frames, nine dome flats in each filter, and three sky flats in each filter on every night of observing.

3. DATA PROCESSING

3.1. Image Reduction

Data were processed using the IRAF data reduction package (Tody 1986). First, a single bias value, determined from the median value in the overscan region of each image, was subtracted from all object and calibration frames. The bias frames were median filtered and fitted with a smooth polynomial that was subtracted from all object and flat-field images. Individual dome and sky flats in each filter were median stacked, and the resulting sky flats processed with the dome flats. The remaining large-scale structure was smoothed, and this smooth correction was recombined with the dome flats to create a master flat-field image for each filter.

These master flat-field corrections were applied to all target and standard-star frames. After this procedure there were still noticeable large-scale gradients in the CCD illumination pattern, especially in the *g* frames. To remove this, we generated dark-sky flat-field frames (also known as illumination corrections) by median filtering all the unregistered target frames in each filter. On those nights when too few targets were observed to generate such an illumination correction, data were combined with an adjacent night. These combined images were smoothed with a large (50 pixel) boxcar, and the resulting correction was applied to both the target and standard-star frames. This procedure results in images that are flat to the $\sim 1\%$ level. Finally, for CCD13, it was necessary to apply a fringe correction to the *i* images. This was generated by median stacking the completely flat-fielded *i*-band target images and smoothing the result with a small (5 pixel) boxcar. The resulting image was used as the fringe correction for the target frames.

3.2. Photometric Calibration

Standard-star photometry was performed using the APPHOT package in IRAF. Stars were photometered in numerous apertures up to 50 pixels (18''.5) in radius, and the local sky was determined using a 10 pixel-wide annulus centered on each star, starting at a radius of 50 pixels. The convergence magnitudes for all three exposures of each star on each frame were measured, and the three values averaged to provide a mean instrumental magnitude.

The resulting collection of between five and 12 measured instrumental magnitudes was used to determine the zero-point offset, air-mass term, and color term in each filter. We used the IRAF FITPARAMS task to fit the relation

$$m_{\text{true}} = m_{\text{inst}} + A + B \sec z + C(\text{color}) \quad (1)$$

TABLE 1
CCD13 EXTINCTION AND COLOR TERMS

Filter	Air Mass	Color
<i>g</i>	-0.152	0.150(<i>g</i> - <i>r</i>)
<i>r</i>	-0.094	0.068(<i>g</i> - <i>r</i>)
<i>i</i>	-0.070	-0.013(<i>g</i> - <i>i</i>)

for each filter. On some nights, not enough standards were observed to robustly determine values for all three unknowns. In these cases, the air-mass and color terms were fixed at those derived from the mean values from nights with sufficient standards (given in Table 1), and only the zero point was determined. Typical rms deviations in the fit of the calibration relation are 0.01 mag. In addition, on two nights, over twenty Gunn standards were observed to test our measurements of the air-mass and color terms. In both cases, the derived terms were within 10% of the mean values derived from other nights with many fewer standards.

3.3. Object Detection and Photometry

Object detection on the target frames was done using the FOCAS package (Jarvis & Tyson 1979; Valdes 1982). The *g*, *r*, and *i* frames were processed independently, using detection parameters of 2.5σ pixel $^{-1}$, a 25 pixel minimum area, and a sky value estimated individually for each image. Object classification was also performed by FOCAS, and the classifications were visually inspected. Bright objects

TABLE 2
PHOTOMETRIC RESIDUALS AT $m_r = 20.0$ mag

Comparison	σ_g	σ_r	σ_i
CCD16 vs. CCD16.....	0.19	0.13	0.09
CCD13 vs. CCD16.....	0.10	0.09	0.10
CCD13 vs. CCD13.....	0.12	0.10	0.16

with incorrect classifications (usually due to saturated pixels) were corrected by hand. The photometric coefficients derived from the standard-star observations were used to determine object magnitudes. The color terms were applied only after objects were detected in multiple filters, and then the images were matched up at a later stage. For objects detected in only one filter, the default colors $g - r = 0.5$ and $g - i = 0.5$ were used when applying the color correction. To properly study such a large collection of imaging data, we must establish photometric consistency between many observing nights, and in our case, two different detectors. Photometric accuracy is also necessary for using these data to calibrate DPOSS. To examine this question, we observed 51 clusters on two or more occasions. In some cases, both sets of observations were taken with the same CCD, and in others, with both CCDs.

We have compared the photometry of numerous multiply observed clusters in three scenarios: (1) both observations with CCD16, (2) one observation with CCD16 and one with CCD13, and (3) both observations with CCD13. We find that there are no systematic night-to-night or CCD-to-CCD photometric offsets greater than 0.05 mag, and the residuals are typically 0.05 mag at $m_{gri} = 19$ mag, rising to no more than 0.15 mag for objects within 1 mag of the detection limit. Table 2 presents the typical residuals at $m_r = 20.0$ mag for the various comparisons, while Figure 1 shows a typical set of photometric comparisons. The left panel compares photometry for the cluster A31, for which both nights of data were taken with CCD16. The data were taken 14 months apart. The middle panel compares photometry for the cluster A98, with one night of CCD16 data and one night of CCD13 data. In this case, the data were taken almost four years apart. Finally, the right panel shows photometry for A2562, with both nights of data taken with CCD13, only 3 months apart. The bottom of each panel shows the magnitude difference between each pair of observations.

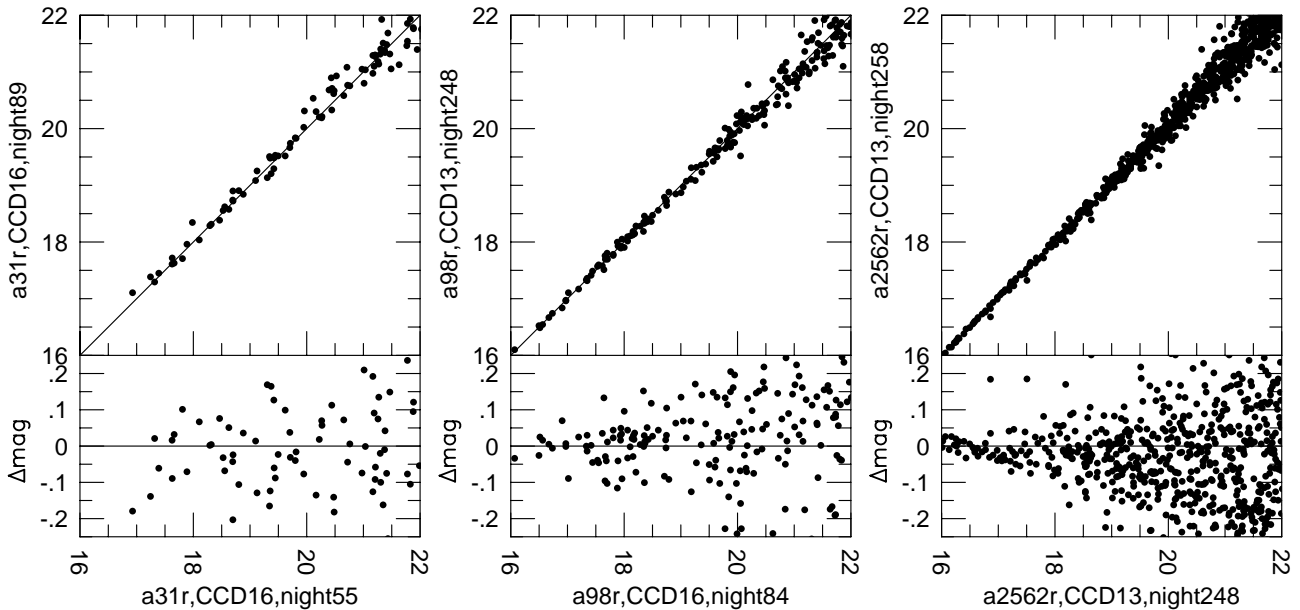


FIG. 1.—Typical photometric comparisons for the cluster A31 (left), for which both nights of data were taken with CCD16, the cluster A98 (middle), with one night of CCD16 data and one night of CCD13 data, and the cluster A2562 (right), with both nights of data taken with CCD13. The bottom of panel shows the magnitude difference between each pair of observations.

4. PHOTOMETRIC REDSHIFTS

From the CCD data, we wish to measure the redshift of each cluster. This can be done either by estimating the redshift of each galaxy individually and examining the resulting redshift distribution or by using the properties of all the galaxies in the image. We have chosen to use the second method, for a number of reasons. First, we have only limited wavelength coverage. Having only three filters (and especially lacking u images) makes it difficult to disentangle color-redshift degeneracies. Second, our photometric errors on individual objects are significant enough to pose a problem for an object-by-object redshift estimator. Finally, since we have performed object detection in the different filters independently (i.e., we do not have matched apertures), there may be systematic effects in the relative colors of different galaxy types. We have therefore elected to use the average properties of the galaxies in each field. Spectroscopic redshifts are taken from Struble & Rood (1991, 1999).

4.1. Deriving the Relation

We estimate the redshift by assuming that each field contains a single cluster at one redshift and that the cluster galaxy population is dominated by early-type galaxies. The $g - r$ color of elliptical galaxies evolves rapidly at $z < 0.4$ because of a strong k -correction, as the 4000 Å break passes through the g filter. Similarly, the g magnitudes of these galaxies fade rapidly with redshift because of both distance and k -correction effects. For these reasons, we have chosen to use the $g - r$ colors and g magnitudes of the cluster galaxies in our photometric redshift estimator. The assumption of a single cluster per CCD field is reasonable, although projections are certain to occur. While it has been estimated that up to 35% of clusters in the Abell catalog with $R \geq 1$ may be the result of projections of poorer clusters (van Haarlem, Frenk, & White 1997), our results will be dominated by the richest cluster in each field. Our redshift estimator will fail if there are two similarly rich clusters projected along the line of sight.

We count the number of galaxies as a function of color, N_{g-r} , and the number N_g as a function of g aperture magnitude (our aperture has a radius of 13 pixels, or $\sim 5''$) inside each CCD frame imposing a magnitude limit of $m_r = 21.5$ mag for CCD 13 and $m_r = 21.0$ mag for CCD16 to avoid incompleteness. We use the whole CCD area (as opposed to a given physical radius) because the size of our field is comparable to the sizes of clusters in the redshift range we are examining, and the centers of many clusters are not well determined.

First, we apply an extinction correction to the magnitudes and colors of all objects in our fields, derived from the maps of Schlegel, Finkbeiner, & Davis (1998). A single correction is used for each CCD field, since the pixel size of the extinction maps is comparable to the CCD FOV and the vast majority of our fields are at high galactic latitudes; the mean $E(B-V)$ for our sample is 0.075 mag. A statistical background correction must then be applied to both galaxy color and magnitude distributions. These corrections, $N_{bg,g-r}$ and $N_{bg,g}$, are determined from a set of 22 observations of random fields taken with CCD13 during numerous observing runs. This distribution (scaled to the appropriate area for CCD16 data), is then subtracted from the color and magnitude distributions of each cluster, and

the median $g - r$ color and mean g magnitude of the remaining galaxies are calculated. An example showing this procedure is shown in Figure 2. The thin solid line is the distribution of all galaxy colors $g - r$ in CCD13 images of Abell 2063. The dotted line is the distribution of galaxy colors derived from our random field observations, while the thick solid line is the background-corrected distribution. A sharp peak at $g - r \sim 0.5$ is seen, corresponding to the early-type galaxy population in this cluster.

Empirical relations between our measured cluster properties and the spectroscopic redshifts were then derived independently for CCD13 and CCD16 data. For CCD13, 114 clusters with measured redshifts were used, while only 33 clusters were available for use with CCD16. Using the GAUSSFIT package (Jefferys, Fitzpatrick, & McArthur 1987), we performed a bivariate least-squares fit, deriving the following relations between redshift, median $g - r$ color, and mean g magnitude:

Using CCD13 with $m_{r,lim} = 21.5$,

$$\log z = 3.2619(g - r)_{\text{med}} - 1.6687(g - r)_{\text{med}}^2 + 0.1190g_{\text{mean}} - 4.6532 ; \quad (2)$$

and using CCD16 with $m_{r,lim} = 21.0$,

$$\log z = 3.2151(g - r)_{\text{med}} - 1.6957(g - r)_{\text{med}}^2 + 0.0710g_{\text{mean}} - 3.5983 . \quad (3)$$

The formal errors on each coefficient from the fit are very small (± 0.0002 or less). The above relations, although apparently dissimilar, should be universal, since we are using calibrated quantities. To test this, we applied the same magnitude cut ($m_r < 21.0$) used for the CCD16 data to the CCD13 data. The coefficients from the CCD16 fit were then used to estimate redshifts for the CCD13 clusters with spectroscopic redshifts. The rms of $z_{\text{spect}} - z_{\text{PHOT}}$ was only marginally higher (0.025 vs. 0.024) than that using the true CCD13 fit, although a slight systematic overestimate of the

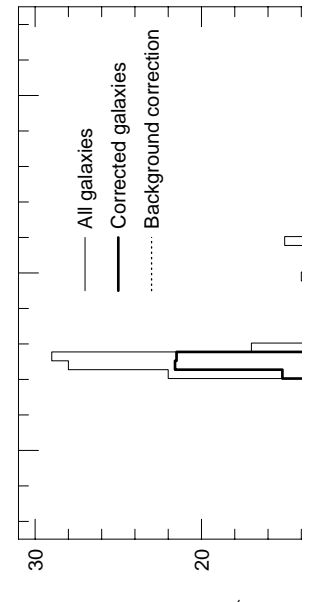


FIG. 2.—Example of the background correction procedure showing the distribution of all galaxy colors $g - r$ in CCD13 images of Abell 2063 (thin solid line), the distribution of galaxy colors derived from our random field observations (dotted line), and the background-corrected distribution (thick solid line). A sharp peak at $g - r \sim 0.5$ is seen, corresponding to the early-type galaxy population in this cluster.

redshift does occur at $z < 0.1$. The effects of detector area, the background correction technique, and the sample used can all affect the fit; nevertheless, it appears that our derived relations should be applicable to other data sets treated in an identical fashion (i.e., same filters, apertures, magnitude cuts, and background correction).

It is important to note that the combination of both color and magnitude information significantly improves our photometric redshift estimates. Figure 3 shows the photometric redshift estimates using magnitudes only, colors only, and the combination of colors and magnitudes for the CCD13 data. The scatter in redshift decreases from 0.034 for magnitudes only, to 0.031 for colors only, to 0.024 when both are used.

4.2. Redshift Errors

The rms of $z_{\text{spec}} - z_{\text{phot}}$ are $\sigma(z) = 0.024$ and 0.027 for CCD13 and CCD16, respectively. These figures represent the intrinsic scatter of our derived relationship between redshift and photometric properties. The scatter is larger for

the CCD16 data because of the small number of clusters with spectroscopic redshifts used in the derivation. The error on any individual cluster redshift depends not only on the scatter of the relation, but also on the number of clusters in the local redshift range used to determine the relation. For instance, at the high-redshift end ($z \sim 0.3$), there are only four clusters that constrain the relation for the CCD13 data. Therefore, we expect the errors in this redshift range to be larger than those at $0.05 < z < 0.1$, for which there are 29 clusters.

To estimate the magnitude of this effect, we have performed bootstrap simulations of our training samples. We randomly select, with replacement, clusters from our training sample until we have built a new training sample of the same size as the original (114 for CCD13, 33 for CCD16). This new sample is used to derive a new redshift estimator, which is then applied to the original sample. We repeat this procedure 500 times for each cluster and calculate the mean redshift estimate and the standard deviations about this estimate. Figure 4 shows the photometrically estimated red-

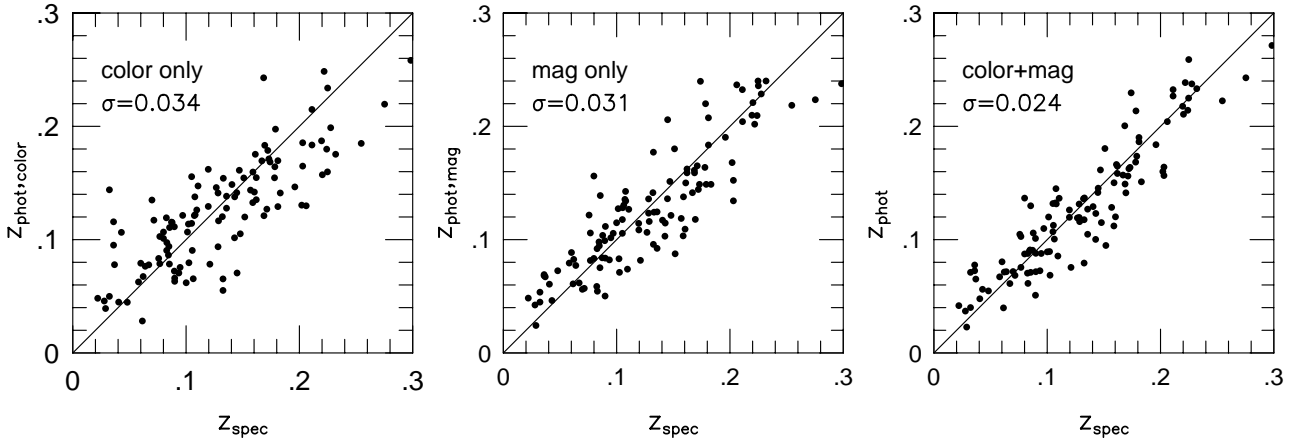


FIG. 3.—Photometric redshift estimates for the CCD13 data plotted against the spectroscopic redshifts, using magnitudes only, colors only, and the combination of colors and magnitudes to derive the estimates. The decrease in scatter is clearly seen.

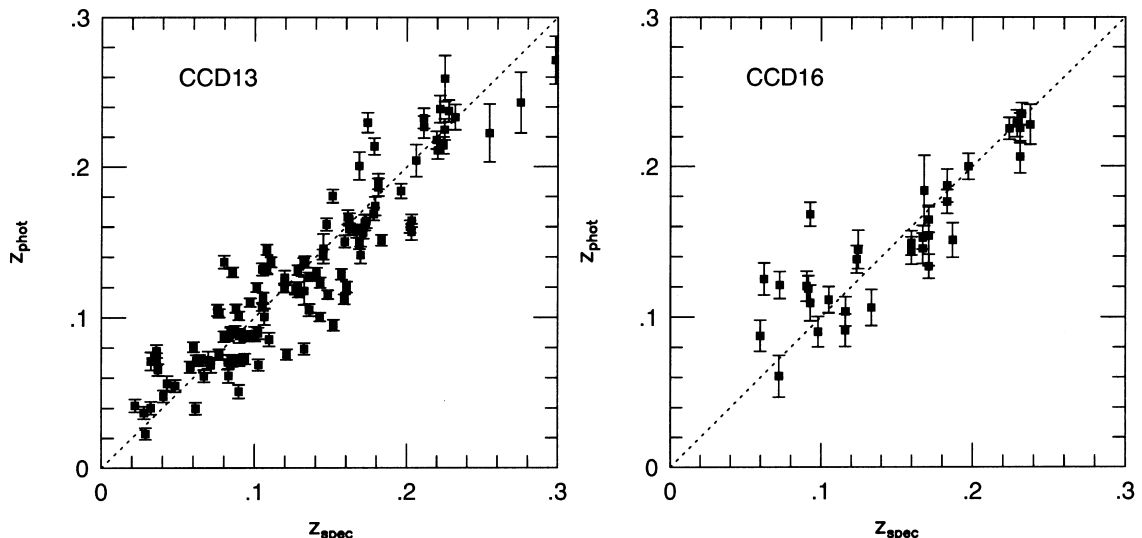


FIG. 4.—Photometrically estimated redshift against the spectroscopically measured redshift for both CCDs. Error bars on individual redshifts represent the 1σ redshift limits from the bootstrap procedure. The 114 clusters used to derive the relation for CCD13 are on the left, while the 33 clusters used for CCD16 are on the right.

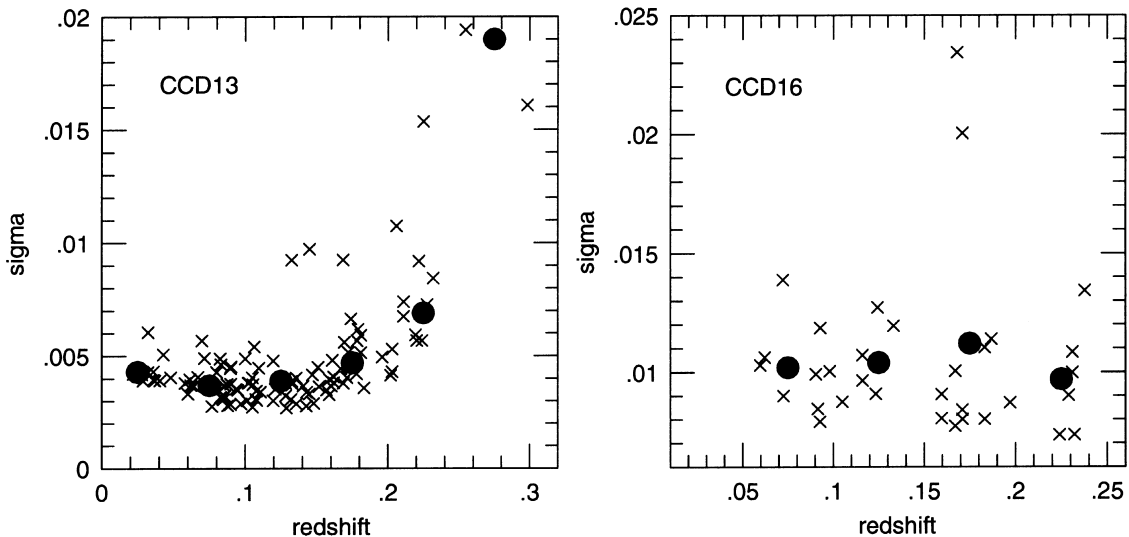


FIG. 5.—Error of each cluster redshift as determined by our bootstrap simulation (crosses) and mean redshift errors in redshift bins of $\Delta z = 0.05$ (circles). The left panel shows the 114 clusters from CCD13, while the right panel shows the 33 clusters from CCD16.

shift against the spectroscopically measured redshift for both CCDs. Error bars on individual redshifts represent the 1σ redshift limits from the bootstrap procedure.

Clearly, the errors are smallest in the redshift bins with the largest number of calibrating clusters. Figure 5 shows the errors on each cluster redshift derived from the bootstrap procedure. Circles show the mean redshift errors in bins of $\Delta z = 0.05$. For CCD13, the errors are largest at $z \sim 0.3$, where there are only three clusters. The redshift distribution for CCD16 clusters is more even, yielding nearly equal errors over the entire redshift range. To estimate the true redshift error on any given measurement, we add in quadrature the intrinsic scatter of our z_{PHOT} versus z_{spec} relation, and the error from the appropriate bin from our bootstrap simulation. This error estimate then encompasses both the intrinsic errors of our fit and the errors introduced from our sample selection. For 57 clusters we have multiple observations from which to estimate their redshifts. Comparing these redshift estimates, we find rms $\Delta z = 0.038$, which is exactly what we expect from the individual error estimates. Our redshift errors are not dominated by photometric errors, since a large number of galaxies contribute to the mean color and magnitude values in each cluster. The scatter is most likely due to inaccurate spectroscopic redshifts (less than 20% of the clusters have three or more galaxies with measured redshifts) and variance in the cluster properties (such as blue galaxy fraction, and richness). For instance, Miller et al. (1999) have demonstrated that projection effects have resulted in significantly erroneous redshifts for 14% of clusters with single spectroscopic redshifts. These two effects cannot be disentangled without a larger sample of clusters with properly measured spectroscopic redshifts. Unfortunately, almost all of the clusters we studied that also have a significant number of spectroscopic redshifts are very nearby ($z < 0.05$), and therefore we cannot draw any significant conclusions about spectroscopic redshift errors for our sample as a whole.

We present the photometric results in Table 3. Clusters are arranged in numerical order. Column (1) lists the Abell cluster number. Column (2) lists the CCD used for the

observation. Columns (3)–(4) provide the background-corrected median $g - r$ color and g magnitude for each cluster. Column (5) lists the extinction, $E(B - V)$. Column (6) provides the photometric redshift estimate, and column (7) contains the estimated error, as described above. The final column lists the spectroscopic redshift, if it is available. For clusters with very low spectroscopic redshifts ($z_{\text{spec}} < 0.03$), we usually obtain a significantly higher photometric redshift. For these clusters, our CCD field covers only a small physical area, and we are likely seeing through the lower redshift cluster and measuring a background cluster.

5. DISCUSSION AND FUTURE WORK

This paper presents the data acquisition, reduction, and photometric analysis of an unprecedented sample of CCD *gri* observations of Abell clusters. We have demonstrated the photometric consistency of our sample and presented a simple yet effective photometric redshift estimator. A total of 431 clusters have been studied, providing 236 new photometric redshift estimates. In addition, we have shown our photometric redshift estimator to be universal. The derived relations between redshift, colors, and magnitudes can be applied to any other data set taken with the same filters and analyzed in an identical way.

These new redshifts enable a variety of projects for which photometry alone is not sufficient and distance information is required, but high accuracy is not necessary. The evolution of galaxy and cluster properties with time (such as the Butcher-Oemler effect, morphology-density relation, and luminosity functions) are prime examples of such science. In addition, these photometric redshifts are a useful check on the spectroscopic redshifts of galaxy clusters, many of which are derived from a single measured galaxy.

Future papers will use a large sample to perform large, statistical studies of low-redshift ($z < 0.3$) galaxy clusters. The next paper will discuss the Butcher-Oemler effect (as was done for a smaller sample by Margoniner & de Carvalho 2000), and later papers will measure luminosity functions and study intracluster light, the color-magnitude relation, the Binggeli effect (Binggeli 1982), and galaxy morphology. Bringing in data from other wavelengths, most

TABLE 3
CLUSTER PROPERTIES AND PHOTOMETRIC REDSHIFTS

Abell (1)	CCD (2)	$g - r_{\text{med}}$ (3)	g_{mean} (4)	$E(B - V)$ (5)	z_{phot} (6)	Error (7)	z_{spec} (8)	Abell (1)	CCD (2)	$g - r_{\text{med}}$ (3)	g_{mean} (4)	$E(B - V)$ (5)	z_{phot} (6)	Error (7)	z_{spec} (8)
21	13	0.56984	19.1749	0.03911	0.0881	0.0243	0.0946	262.....	13	0.55546	18.2927	0.09019	0.0598	0.0243	0.0163
26	13	0.68976	19.8172	0.06752	0.1448	0.0243	0.1449	272.....	13	0.57489	19.7996	0.04788	0.1062	0.0243	0.0877
31	16	0.62472	19.9006	0.03836	0.1452	0.0289	0.1596	275.....	16	0.86527	20.2964	0.05229	0.2268	0.0287	...
54	13	0.65092	19.7028	0.03686	0.1498	0.0289	0.1596	278.....	13	0.56409	19.7509	0.05465	0.1013	0.0243	0.0891
59	13	0.75757	20.4157	0.04703	0.1947	0.0245	...	288.....	13	0.70207	19.6760	0.06845	0.1430	0.0243	...
60	13	0.71243	20.1403	0.05342	0.1660	0.0245	...	300.....	16	0.71702	19.5644	0.1431	0.0243
62	16	0.50123	19.4658	0.03938	0.0933	0.0289	...	307.....	13	0.72066	20.2539	0.05813	0.1890	0.0292	...
65	16	0.78512	20.0763	0.06377	0.2026	0.0287	0.1206 ^a	311.....	13	0.94115	19.4678	0.09527	0.00551	0.0244	...
68	13	1.11481	20.5031	0.09476	0.2233	0.0250	0.2546	318.....	13	0.65820	19.8653	0.06498	0.1363	0.0243	0.1320
69	13	0.64688	20.1062	0.05788	0.1415	0.0243	0.1454	320.....	13	0.91160	20.1860	0.08404	0.2165	0.0250	...
73	16	0.84825	19.2846	0.05788	0.1899	0.0292	0.1454	330.....	13	0.58288	20.2481	0.09242	0.1231	0.0243	...
79	13	1.05318	20.3368	0.09367	0.2244	0.0250	...	333.....	16	0.70736	19.9066	0.09204	0.1759	0.0292	...
82	16	0.69633	19.7945	0.08488	0.1676	0.0292	0.0927 ^a	345.....	13	0.61722	19.2636	0.16864	0.1038	0.0243	...
83	16	0.64521	19.4615	0.03514	0.1181	0.0243	...	347.....	13	1.09518	17.3148	0.05747	0.0950	0.0243	0.0184
98	13	0.57916	19.7885	0.04508	0.1073	0.0243	0.1050	349.....	13	0.57984	19.3553	0.06075	0.0955	0.0243	...
110	13	0.49108	19.4000	0.04784	0.0715	0.0243	0.1050	360.....	13	0.85185	20.2633	0.07576	0.2116	0.0250	0.2205
115	16	0.90548	19.3913	0.05764	0.1995	0.0292	0.1971	364.....	13	0.66718	20.1751	0.16586	0.1516	0.0245	0.1800 ^b
136	16	0.90075	20.5781	0.05666	0.2418	0.0287	0.1569	372.....	13	0.64544	19.8768	0.09561	0.1324	0.0243	0.1073
137	16	0.58929	19.6325	0.06651	0.1264	0.0289	0.1136	373.....	13	0.63530	19.4034	0.15390	0.1486	0.0243	...
142	16	1.19339	20.3110	0.02611	0.1846	0.0292	0.1050	374.....	13	0.66272	20.1405	0.15390	0.1113	0.0243	...
143	16	0.64219	20.2976	0.07644	0.1617	0.0292	0.0679	376.....	13	0.61523	19.3218	0.05121	0.1049	0.0243	0.0757
152	13	0.51463	18.8969	0.03561	0.0679	0.0243	0.0581	377.....	13	0.49633	18.3979	0.07008	0.0554	0.0243	0.0481
153	13	0.61917	20.1015	0.03076	0.1313	0.0243	0.1279	378.....	13	0.74239	19.7053	0.14500	0.1937	0.0245	...
154	13	0.50904	19.1955	0.06283	0.0722	0.0243	0.0624	397.....	13	0.575779	20.3970	0.14423	0.1560	0.0245	...
163	16	0.62253	20.2190	0.05280	0.1532	0.0292	...	399.....	13	0.63978	19.6092	0.22645	0.1275	0.0243	...
165	13	0.60361	19.7734	0.05807	0.1149	0.0243	...	408.....	13	0.57552	19.7137	0.05816	0.1040	0.0243	...
167	16	0.68404	20.3669	0.05187	0.1795	0.0292	0.1279	382.....	13	0.97386	20.3809	0.04618	0.2356	0.0287	...
175	13	0.47652	19.4959	0.03076	0.1196	0.0243	0.1243	384.....	16	0.51087	19.3063	0.15054	0.0405	0.0244	0.0327
191	13	0.90729	20.6865	0.06023	0.2477	0.0250	0.0243	411.....	16	0.40766	18.5634	0.16449	0.0686	0.0243	0.0724
196	13	0.701350	20.1011	0.07062	0.2117	0.0250	...	429.....	13	0.50475	19.8261	0.16449	0.0686	0.0243	...
219	13	0.670417	18.9628	0.07354	0.1182	0.0243	0.1292	421.....	13	0.545026	19.8261	0.16449	0.0686	0.0243	...
227	13	0.67306	20.0422	0.07266	0.1482	0.0243	0.0306	436.....	13	0.52151	18.4605	0.27183	0.0617	0.0243	...
234	13	0.67408	20.3887	0.06394	0.1634	0.0245	0.1731	437.....	13	0.55318	19.4990	0.04673	0.0913	0.0243	0.0847
245	13	0.47259	19.1110	0.05571	0.0616	0.0243	0.0790 ^b	439.....	13	0.63436	18.9645	0.18273	0.1354	0.0243	0.1068
246	13	0.53622	18.6123	0.06930	0.0677	0.0243	0.0700 ^b	444.....	13	0.66930	19.2705	0.36639	0.1189	0.0243	...
247	16	0.70622	19.9252	0.05394	0.1745	0.0292	...	452.....	13	0.72971	18.7953	0.36592	0.0597	0.0243	...
249	13	0.69410	20.6258	0.07400	0.1824	0.0245	...	461.....	13	0.94078	19.9688	0.09804	0.0884	0.0243	...
253	13	0.85473	20.4095	0.07359	0.2208	0.0250	0.0250	465.....	13	0.65280	19.7421	0.26737	0.1300	0.0243	0.1300 ^b
257	16	0.61246	19.6717	0.05504	0.1355	0.0289	0.0243	468.....	13	0.55633	18.9604	0.18108	0.0796	0.0243	0.1325
258	13	0.09506	18.7597	0.10749	0.0111	0.0244	...	477.....	13	0.73595	18.7085	0.1174	0.0243	0.0245	...
260	13	0.15118	18.8687	0.10749	0.0075	0.0244	...	477.....	13	0.92203	20.5368	0.19900	0.2394	0.0250	...
260	13	0.48142	19.2192	0.04944	0.0656	0.0243	0.0369	478.....	13	1.13313	20.2364	0.19900	0.2033	0.0250	...
260	13	0.48142	19.2192	0.04944	0.0656	0.0243	0.0369	478.....	13	0.59300	18.9106	0.50950	0.0880	0.0243	0.0881 ^b

TABLE 3—Continued

Abell	CCD	$g - r_{\text{med}}$	g_{mean}	$E(B-V)$	z_{phot}	Error	z_{spec}	Abell	CCD	$g - r_{\text{med}}$	g_{mean}	$E(B-V)$	z_{phot}	Error	z_{spec}
(1)	(2)	(3)	(4)	(5)	(6)	(7)	(8)	(1)	(2)	(3)	(4)	(5)	(6)	(7)	(8)
485.....	13	0.73114	19.6791	0.19952	0.1517	0.0245	...	688.....	13	0.661148	19.9358	0.02399	0.1401	0.0243	...
497.....	13	0.53289	18.8471	0.33775	0.0716	0.0243	...	696.....	13	0.666665	20.2914	0.02464	0.1563	0.0245	...
498.....	13	0.54786	18.3495	0.40129	0.0655	0.0243	...	699.....	13	0.50383	19.2307	0.05015	0.0716	0.0243	0.0851
501.....	13	0.53364	19.8623	0.20177	0.0952	0.0243	0.1517	706.....	13	0.68127	20.7678	0.05126	0.1843	0.0245	...
502.....	13	0.47876	17.9496	0.16282	0.0465	0.0244	...	710.....	13	0.82540	20.8878	0.03391	0.2441	0.0250	...
504.....	13	0.53374	19.0054	0.13891	0.0757	0.0243	...	715.....	13	0.70071	20.9068	0.03819	0.1998	0.0245	0.1685
508.....	13	0.61470	19.6654	0.13706	0.1151	0.0243	0.1479	720.....	13	1.03609	20.8913	0.03034	0.2635	0.0306	0.1329 ^a
509.....	13	0.68490	20.2419	0.14506	0.1609	0.0245	0.0836	724.....	16	0.53159	18.5909	0.02975	0.0895	0.0289	0.0933 ^b
515.....	13	0.44215	18.3532	0.09844	0.0443	0.0244	0.0244	732.....	13	0.64268	20.5079	0.04848	0.1637	0.0245	0.2030
520.....	13	0.71559	19.9856	0.04703	0.1601	0.0245	0.1990	734.....	13	0.68154	20.3330	0.04848	0.1563	0.0245	0.2030
523.....	13	0.60029	18.8088	0.14601	0.0891	0.0243	0.1000	741.....	13	0.81491	20.6592	0.03223	0.2264	0.0250	0.0719
525.....	13	0.67672	19.8333	0.13978	0.1412	0.0243	0.0243	749.....	16	0.87969	19.7788	0.02001	0.2102	0.0287	...
526.....	13	0.54725	19.4433	0.09844	0.0882	0.0243	0.0835	750.....	13	0.69543	20.0636	0.04477	0.1568	0.0245	...
529.....	13	0.52781	19.1887	0.08734	0.0770	0.0243	0.0770	750.....	13	0.69561	20.2390	0.04248	0.1583	0.0245	0.1800
530.....	13	0.71692	18.6154	0.07989	0.1103	0.0243	0.0243	752.....	13	0.70324	20.0379	0.04248	0.1646	0.0245	0.1800
532.....	13	0.66337	19.3781	0.21411	0.1209	0.0243	0.0243	752.....	13	0.65009	20.6341	0.02153	0.1565	0.0245	...
537.....	13	0.83142	20.5565	0.13948	0.2244	0.0250	0.0250	755.....	13	0.91807	20.1178	0.02630	0.2131	0.0250	...
539.....	13	0.31046	18.2052	0.16181	0.0232	0.0244	0.0284	759.....	16	0.94435	20.0263	0.01980	0.2228	0.0287	...
541.....	13	1.44808	17.8569	0.19176	0.0496	0.0244	0.0244	779.....	13	0.95530	20.9636	0.01599	0.2715	0.0306	0.0229 ^a
546.....	13	0.83132	19.8455	0.19558	0.1847	0.0245	0.0245	781.....	13	1.02474	20.9976	0.02206	0.2725	0.0306	0.2980
549.....	13	0.99926	20.4647	0.14110	0.2371	0.0250	0.0250	791.....	13	0.79105	20.1921	0.03118	0.1929	0.0245	...
553.....	13	0.46492	19.2178	0.15635	0.0615	0.0243	0.0664	795.....	13	0.54773	20.0723	0.02871	0.1050	0.0243	0.1359
554.....	13	0.54244	19.0158	0.10251	0.0772	0.0243	0.0243	815.....	13	0.62135	19.9541	0.02962	0.1269	0.0243	0.1359
556.....	13	0.65611	18.8411	0.09980	0.1024	0.0243	0.0243	815.....	13	0.90653	20.5706	0.01982	0.2399	0.0250	...
557.....	13	1.37318	19.9090	0.10900	0.1117	0.0243	0.0243	815.....	13	0.62725	20.1492	0.03356	0.1360	0.0243	...
558.....	13	1.17091	18.2115	0.10936	0.0846	0.0243	0.0243	815.....	13	0.61231	20.1526	0.03610	0.1307	0.0243	...
559.....	13	0.57205	19.0006	0.10936	0.0105	0.0244	0.0244	815.....	16	1.26743	20.9694	0.01711	0.1746	0.0292	0.4069
567.....	13	0.59490	19.8080	0.11074	0.1131	0.0243	0.0243	815.....	13	0.75560	20.4164	0.01970	0.1940	0.0245	...
569.....	13	0.60708	20.1740	0.11074	0.1295	0.0243	0.0243	815.....	16	0.90464	20.6850	0.01030	0.2464	0.0287	...
574.....	13	0.61141	19.0390	0.07508	0.0961	0.0243	0.0201	937.....	13	0.56146	19.9056	0.04112	0.1048	0.0243	...
574.....	13	0.96262	20.3645	0.03163	0.2309	0.0250	0.1740	942.....	13	0.58843	20.1755	0.01418	0.1227	0.0243	...
579.....	16	0.60821	19.5383	0.06554	0.1311	0.0289	0.0289	954.....	16	0.59112	19.3193	0.03458	0.1207	0.0289	0.0932
580.....	13	0.47746	19.7908	0.07691	0.0756	0.0243	0.0243	957.....	16	0.87561	19.4017	0.03351	0.1971	0.0292	0.0450 ^a
583.....	16	0.66862	20.0568	0.06291	0.1651	0.0292	0.0292	967.....	16	0.84000	20.1400	0.01359	0.2169	0.0287	...
586.....	16	0.67197	19.9786	0.05758	0.1642	0.0292	0.1710	969.....	16	0.50442	18.8411	0.03372	0.0852	0.0289	...
587.....	13	0.55457	19.9488	0.06260	0.1038	0.0243	0.1680	986.....	13	0.85127	20.6757	0.04148	0.2368	0.0250	...
590.....	13	0.53404	20.0988	0.05466	0.1010	0.0243	0.0243	1015.....	13	1.29165	20.5934	0.01384	0.1684	0.0245	...
611.....	13	0.61826	20.3126	0.04781	0.1388	0.0243	0.2880	1019.....	16	0.72710	20.3142	0.01938	0.0292	0.0245	...
630.....	13	0.59567	19.3910	0.02951	0.1011	0.0243	0.0243	1030.....	16	0.85723	20.3117	0.01841	0.2261	0.0287	0.1780 ^b
635.....	13	0.69993	20.6623	0.04882	0.1865	0.0245	0.0245	1034.....	13	0.72808	20.0985	0.01671	0.1123	0.0243	0.1585
647.....	13	0.46777	19.3110	0.04504	0.0638	0.0243	0.0243	1095.....	16	0.58365	19.3148	0.01948	0.1188	0.0289	0.1208 ^b
657.....	13	0.86745	20.5141	0.02353	0.2299	0.0250	0.0250	1095.....	13	0.76750	20.5136	0.03201	0.2033	0.0250	...
665.....	13	0.606363	19.7952	0.02951	0.0080	0.0244	0.0244	1095.....	13	0.68803	20.2837	0.04027	0.1639	0.0245	...
668.....	13	0.59567	19.8627	0.04360	0.0487	0.0244	0.1819	1101.....	16	0.92782	20.3118	0.01740	0.2331	0.0287	0.2322
668.....	13	0.55004	19.6021	0.05564	0.1621	0.0245	0.1819	1114.....	13	0.47207	20.1248	0.02872	0.0811	0.0243	0.0140
677.....	13	0.70330	21.1855	0.04541	0.2430	0.0250	0.0250	1120.....	13	0.79550	20.9401	0.02972	0.2383	0.0250	0.2218
687.....	13	1.10518	20.7766	0.04360	0.2168	0.0250	0.0250	1140.....	13	1.17952	20.9944	0.01990	0.2347	0.0250	...
687.....	13	0.94758	20.5253	0.02483	0.2407	0.0250	0.0250	1299.....	13	0.41872	20.1729	0.02565	0.0661	0.0243	0.2247

TABLE 3—Continued

Abell (1)	CCD (2)	$g - r_{\text{med}}$ (3)	g_{mean} (4)	$E(B - V)$ (5)	z_{phot} (6)	Error (7)	z_{spec} (8)	Abell (1)	CCD (2)	$g - r_{\text{med}}$ (3)	g_{mean} (4)	$E(B - V)$ (5)	z_{phot} (6)	Error (7)	z_{spec} (8)	
1345	13	0.50007	19.9364	0.04435	0.0856	0.0243	0.1095	1889	16	0.43053	19.5939	0.01446	0.0730	0.0289	0.1860 ^b	
1356	13	0.44753	20.0358	0.04992	0.0718	0.0243	0.0698	1900	16	0.73368	19.3106	0.01198	0.1657	0.0292	0.1718 ^b	
1413	13	0.57322	19.6151	0.02308	0.1005	0.0243	0.1427	1905	13	0.90926	20.2457	0.01967	0.2386	0.0250	0.3392 ^b	
1441	13	0.56523	19.5451	0.01963	0.0961	0.0243	0.1399	1909	13	0.6985	18.7493	0.02100	0.0217	0.0244	0.1456 ^a	
1445	13	0.60697	20.4888	0.02511	0.1411	0.0243	0.1694	1914	13	0.70911	19.9440	0.02253	0.1562	0.0245	0.1712	
1475	13	0.71660	20.7940	0.03053	0.2002	0.0250	0.1917	1917	13	0.65633	20.7987	0.03411	0.1753	0.0245	...	
1481	13	0.646412	20.1934	0.03169	0.0801	0.0243	0.1569	1926	13	0.45225	19.0446	0.02335	0.0558	0.0243	0.1338	
1487	13	0.80138	20.7258	0.01770	0.2265	0.0250	0.2111	1934	13	0.81717	20.5205	0.01296	0.2185	0.0250	0.2194	
1489	13	1.03265	19.9782	0.02366	0.2055	0.0250	0.2060	1954	13	0.49161	20.5259	0.01765	0.0976	0.0243	0.1810	
1495	13	0.59984	20.0652	0.02300	0.1231	0.0243	0.1429	1965	16	1.33724	20.8859	0.01321	0.1213	0.0289	...	
1497	13	0.65830	20.3739	0.02513	0.1567	0.0245	0.1669	1967	16	1.39209	21.0136	0.01321	0.1420	0.0289	...	
1499	13	0.60883	20.1277	0.03933	0.1285	0.0243	0.1569	1979	13	0.69590	19.8762	0.01644	0.1491	0.0243	0.1687	
1526	13	0.52537	19.6862	0.04942	0.0875	0.0243	0.0800	1987	16	0.60901	19.0374	0.01949	0.1210	0.0289	...	
1551	16	0.70359	19.6431	0.01295	0.1658	0.0292	0.1319 ^b	1987	16	0.83691	20.4901	0.02416	0.2217	0.0250	0.1269	
1577	13	0.59981	19.8800	0.02463	0.1170	0.0243	0.1409 ^b	1990	13	1.39209	21.0136	0.01321	0.1420	0.0289	...	
1578	16	0.63441	19.1858	0.02452	0.1323	0.0289	0.2005	2005	16	0.65914	19.1451	0.02643	0.1393	0.0289	...	
1592	16	0.86737	20.3286	0.01626	0.2283	0.0287	0.2008	2008	13	0.75044	20.3750	0.05147	0.1902	0.0245	0.1810	
1608	16	0.73723	19.3522	0.01494	0.1678	0.0292	0.1319 ^b	2016	13	0.65029	20.2297	0.04019	0.1477	0.0243	...	
1613	16	0.67606	19.7880	0.01833	0.1606	0.0292	0.1608 ^b	2017	13	0.62659	20.1667	0.04933	0.1364	0.0243	0.1187	
1620	13	0.455548	19.8524	0.02533	0.0705	0.0243	0.0821	2034	16	0.68979	18.7973	0.01520	0.1405	0.0289	0.1130 ^b	
1647	16	0.78172	19.9377	0.02458	0.1972	0.0292	0.2042	2042	16	0.59510	19.7934	0.01658	0.1319	0.0289	0.2353 ^a	
1656	13	0.42058	18.5126	0.00840	0.0423	0.0243	0.0231	2063	13	0.66303	19.9529	0.03458	0.1412	0.0243	0.0353 ^a	
1657	16	0.77811	19.6795	0.02757	0.1881	0.0292	0.2065	2065	16	0.39157	19.3454	0.04122	0.0595	0.0289	0.0726	
1661	16	0.66630	19.6312	0.01671	0.1532	0.0292	0.1690	2069	16	0.2346	19.3059	0.0918	0.0289	0.1160	...	
1670	16	0.68407	19.1141	0.01671	0.1463	0.0289	0.1690	2110	16	0.51463	19.0823	0.02508	0.0917	0.0289	0.0980	
1677	16	1.19250	19.5283	0.02222	0.1627	0.0292	0.2111	2111	16	0.97285	20.2236	0.02595	0.2296	0.0287	0.2290	
1680	13	0.48350	19.8260	0.01743	0.0781	0.0243	0.1820	2116	13	1.29418	20.4549	0.03000	0.1611	0.0245	0.1656 ^b	
1694	16	0.82213	19.9190	0.01146	0.2058	0.0287	0.2126	2126	13	0.71284	20.4204	0.06225	0.1793	0.0245	...	
1711	13	0.64982	19.7342	0.02744	0.0723	0.0243	0.0821	2129	13	0.74726	20.3378	0.05130	0.1872	0.0245	...	
1712	16	0.87111	19.1111	0.01231	0.2457	0.0287	0.2141	2141	16	0.60366	20.0573	0.02138	0.1410	0.0289	0.1584 ^b	
1714	16	0.96882	20.6158	0.01342	0.2242	0.0287	0.2147	2147	13	0.79995	19.6468	0.02125	0.1923	0.0292	0.1584 ^b	
1746	13	1.09522	20.5804	0.01342	0.2450	0.0287	0.2152	2152	13	0.48392	19.8084	0.03332	0.0727	0.0243	0.0350	
1747	13	0.64266	20.0143	0.01437	0.1365	0.0243	0.1947	2155	13	0.48680	19.5180	0.03332	0.0779	0.0243	0.0350	
1748	13	1.01227	19.7564	0.00958	0.1947	0.0245	0.2157	2157	13	0.41326	19.6833	0.04018	0.0565	0.0243	0.0410	
1752	13	0.44244	18.8809	0.02792	0.0513	0.0243	0.0287	2157	13	1.17570	20.4862	0.06581	0.2054	0.0250	0.2465 ^b	
1759	16	1.09547	19.6304	0.01207	0.1561	0.0292	0.1680	2159	13	0.10487	20.2743	0.01809	0.2743	0.0306	...	
1760	16	0.61888	19.5574	0.02926	0.1352	0.0289	0.1711	2177	13	0.767667	20.4227	0.03891	0.1659	0.0245	0.1610	
1785	13	0.60443	20.1930	0.01169	0.1292	0.0243	0.2136	2178	16	0.80138	20.2053	0.03127	0.0727	0.0243	0.0350	
1795	16	0.57284	19.9279	0.01240	0.1266	0.0289	0.0631	2182	16	0.43867	20.1324	0.03728	0.0711	0.0243	0.0322	
1799	13	0.53579	20.5101	0.01115	0.1137	0.0243	0.170	2182	16	0.49221	19.2521	0.08171	0.0690	0.0243	0.1030	
1810	16	0.68330	19.5209	0.01207	0.1561	0.0292	0.1680	2183	13	0.45168	20.0398	0.04102	0.0731	0.0243	...	
1813	16	0.54633	19.0667	0.01668	0.1015	0.0289	0.0947 ^b	2185	13	0.86845	20.3751	0.01547	0.2215	0.0250	...	
1820	13	0.81117	20.6951	0.02743	0.2275	0.0250	0.2196	2186	16	0.53237	19.8593	0.05602	0.1105	0.0289	0.0928	
1821	16	0.61573	19.3145	0.01523	0.1289	0.0289	0.2188	2188	16	0.47559	20.1565	0.0952	0.0289	0.1087	...	
1826	16	0.86756	19.8284	0.01636	0.2104	0.0287	0.2451	2189	16	0.61924	20.2626	0.01013	0.1519	0.0292	0.1875	
1856	13	0.56361	20.5709	0.01695	0.1267	0.0243	0.1854 ^b	2190	13	0.45168	20.3919	0.06308	0.1350	0.0243	...	
1874	16	0.73527	19.2227	0.01704	0.1638	0.0292	0.2199	2191	16	0.61337	19.3977	0.01070	0.1067	0.0243	0.0299	
										16	0.56860	19.0855	0.01070	0.1089	0.0289	0.0299

TABLE 3—Continued

Abell (1)	CCD (2)	$g - r_{\text{med}}$ (3)	g_{mean} (4)	$E(B-V)$ (5)	z_{phot} (6)	Error (7)	z_{spec} (8)	Abell (1)	CCD (2)	$g - r_{\text{med}}$ (3)	g_{mean} (4)	$E(B-V)$ (5)	z_{phot} (6)	Error (7)	z_{spec} (8)
2200.....	13	0.70059	20.0345	0.06997	0.1573	0.0245	2316.....	13	0.99357	20.4234	0.09037	0.2346	0.0250	0.2147	
2205.....	13	0.52694	19.80640	0.05611	0.0909	0.0243	0.0876	13	0.89940	20.4905	0.06625	0.2337	0.0250	0.2110	
2215.....	13	0.83647	20.68664	0.02702	0.2339	0.0250	2317.....	13	0.60557	20.1790	0.06819	0.1291	0.0243	0.1405	
2217.....	16	0.67713	19.6565	0.05380	0.1575	0.0292	2318.....	13	0.54066	19.3494	0.11363	0.0841	0.0243	0.0557 ^b	
2219.....	13	0.97399	20.2862	0.02349	0.2262	0.0250	0.2256	13	0.62367	19.7918	0.0988	0.0243	0.1710		
2221.....	13	0.75515	20.2772	0.01248	0.1866	0.0245	0.1019 ^b	13	0.66613	20.2440	0.16135	0.1541	0.0245	...	
2228.....	13	0.67252	19.6874	0.04829	0.1200	0.0243	0.1013	13	0.69446	19.7792	0.25078	0.1447	0.0243	...	
2229.....	13	0.75386	20.3148	0.02118	0.1882	0.0245	...	13	0.66152	19.7576	0.09939	0.1334	0.0243	...	
2238.....	13	0.67963	20.1779	0.01715	0.1562	0.0245	...	13	0.65102	19.4072	0.48845	0.1181	0.0243	...	
2240.....	13	0.74809	20.7689	0.04179	0.2110	0.0250	0.1380	13	0.61473	19.8558	0.08081	0.1213	0.0243	...	
2241.....	16	0.51370	19.5172	0.03004	0.0982	0.0289	...	16	0.38086	19.0358	0.04782	0.0540	0.0289	...	
2243.....	13	0.63968	20.1087	0.02133	0.1390	0.0243	...	13	0.58182	0.1324	0.04858	0.1324	0.0289	...	
2244.....	13	0.57937	19.8780	0.02313	0.1100	0.0243	0.0968	13	0.52112	19.2292	0.05477	0.0761	0.0243	0.1210	
2246.....	13	1.03852	20.8495	0.02377	0.2602	0.0250	0.0250	13	1.04350	20.6513	0.06633	0.2458	0.0250	0.1244	
2251.....	16	0.72084	20.1940	0.04985	0.1873	0.0292	...	16	0.59421	20.4228	0.06633	0.1459	0.0289	0.1244	
2252.....	13	0.79111	20.6880	0.01414	0.2210	0.0250	0.1147	13	0.54219	19.3538	0.06931	0.1050	0.0289	0.1161	
2254.....	13	0.70617	20.2366	0.05330	0.1682	0.0245	0.1780	13	0.73060	20.3196	0.08706	0.1807	0.0245	...	
2255.....	13	0.68960	19.6058	0.02622	0.1366	0.0243	0.0806	13	0.80511	23.874	0.05509	0.2335	0.0250	...	
2256.....	13	0.53847	19.2448	0.04982	0.0811	0.0243	0.0581	13	0.68978	19.8457	0.11891	0.1459	0.0243	...	
2257.....	13	0.62971	19.4428	0.04085	0.1128	0.0243	0.1054	13	0.83569	20.2282	0.05782	0.2061	0.0250	0.0726 ^a	
2261.....	16	0.56827	20.2002	0.04453	0.1306	0.0289	0.2240 ^b	13	0.56365	19.9434	0.07340	0.1067	0.0243	...	
2262.....	13	0.91988	20.5466	0.05507	0.2399	0.0250	...	13	0.73147	20.4833	0.06705	0.1893	0.0245	...	
2263.....	16	0.89261	20.1596	0.05507	0.2251	0.0287	...	13	0.805581	19.0725	0.14370	0.1449	0.0243	0.1450	
2266.....	13	0.60642	20.2462	0.04994	0.1319	0.0243	0.1051	13	0.46280	17.7167	0.05006	0.0405	0.0244	0.0615	
2267.....	13	0.71157	20.3038	0.04183	0.1875	0.0292	0.1671	16	0.74397	20.4617	0.11311	0.2034	0.0287	0.2280	
2268.....	13	0.86400	20.54743	0.02297	0.2313	0.0250	...	13	0.81282	20.4291	0.11562	0.2216	0.0287	0.2280	
2269.....	13	0.73229	20.4696	0.03480	0.1888	0.0245	...	16	0.83911	20.1990	0.07231	0.2189	0.0287	...	
2270.....	16	1.16571	21.0218	0.03386	0.2415	0.0250	...	13	0.72047	20.0539	0.04946	0.1647	0.0245	0.1508 ^b	
2272.....	13	0.62073	20.2334	0.05035	0.1368	0.0243	0.1329	13	0.56837	19.7775	0.07442	0.1035	0.0243	0.1946	
2273.....	13	1.01048	20.7064	0.03138	0.2527	0.0306	...	13	0.81644	20.4615	0.05332	0.2149	0.0250	0.2240	
2274.....	13	1.02809	19.03767	0.1966	0.0245	0.0245	...	16	0.91703	20.0800	0.05322	0.2240	0.0287	0.2240	
2275.....	13	0.52463	19.7815	0.04312	0.0896	0.0243	0.1029	13	0.79625	20.4579	0.06294	0.2186	0.0287	...	
2278.....	13	0.73838	20.6429	0.03667	0.2003	0.0250	...	13	0.62568	19.5082	0.05697	0.1136	0.0243	...	
2279.....	13	0.65266	19.8254	0.07495	0.1330	0.0243	...	13	0.65888	19.8073	0.05697	0.1344	0.0243	...	
2285.....	16	0.43095	19.1077	0.02784	0.0675	0.0289	...	13	0.72784	20.4625	0.05279	0.1869	0.0245	...	
2286.....	13	0.53359	19.62668	0.04234	0.0886	0.0243	...	13	0.64357	20.3016	0.08163	0.1480	0.0243	...	
2288.....	13	0.406314	19.3434	0.03614	0.0896	0.0243	...	13	0.54429	19.6266	0.05859	0.1143	0.0243	...	
2289.....	13	0.88125	19.6091	0.04916	0.2385	0.0250	0.2276	13	0.66671	19.1478	0.05859	0.0918	0.0243	...	
2291.....	13	0.81070	19.9702	0.05685	0.1864	0.0245	0.1810	13	0.655240	20.2949	0.05203	0.1511	0.0245	0.0456	
2292.....	13	0.64847	18.99227	0.04306	0.1047	0.0243	0.1190 ^b	16	0.98668	20.5918	0.12078	0.2430	0.0287	...	
2297.....	13	0.50607	20.0410	0.03817	0.0901	0.0243	...	16	0.53334	19.5092	0.08588	0.1046	0.0289	...	
2300.....	13	0.64421	19.5768	0.07032	0.1216	0.0243	...	16	1.0455	20.6698	0.06104	0.2250	0.0287	...	
2310.....	13	0.63194	19.3653	0.07897	0.1111	0.0243	...	13	0.74243	20.2355	0.06700	0.1804	0.0245	0.1510	
2311.....	13	0.52620	18.9747	0.06498	0.0722	0.0243	0.0890	16	0.63601	20.2324	0.06324	0.1754	0.0292	...	
2314.....	13	0.86960	20.0638	0.07862	0.2035	0.0250	0.2432	13	0.68740	20.2438	0.09827	0.1619	0.0245	...	
2315.....	13	0.52220	19.0739	0.08541	0.0732	0.0243	0.0894	16	0.73938	20.1356	0.06413	0.1915	0.0292	...	

TABLE 3—Continued

Abell (1)	CCD (2)	$g - r_{\text{med}}$ (3)	g_{mean} (4)	$E(B - V)$ (5)	z_{phot} (6)	Error (7)	z_{spec} (8)	Abell (1)	CCD (2)	$g - r_{\text{med}}$ (3)	g_{mean} (4)	$E(B - V)$ (5)	z_{phot} (6)	Error (7)	z_{spec} (8)
2437	13	0.69214	20.2262	0.08662	0.1628	0.0245	...	2562	...	13	0.80266	19.7829	0.06523	0.2218	0.0250
2439	16	0.70738	20.2025	0.06611	0.1830	0.0292	13	0.90301	20.2926	0.06446	0.1753	0.0245
2440	16	0.57093	19.7181	0.08757	0.1216	0.0289	0.0906	2570	...	13	0.53636	18.9403	0.04200	0.0741	0.0243
2443	13	0.64240	19.8860	0.06173	0.1317	0.0243	0.1080	2571	...	16	0.54843	19.5510	0.04538	0.1105	0.0289
2445	13	0.64582	20.3701	0.05318	0.1517	0.0245	...	2574	...	16	0.53587	20.3121	0.05075	0.1203	0.0289
2447	13	0.44196	19.2650	0.09851	0.0568	0.0243	...	2582	...	16	0.60813	19.8203	0.04932	0.1373	0.0289
2449	13	0.62960	20.3519	0.09851	0.1447	0.0243	...	2584	...	13	0.58608	20.3071	0.11019	0.1263	0.0243
2450	13	0.49500	19.6080	0.05987	0.1072	0.0243	...	2590	...	16	0.68153	20.2835	0.03588	0.1762	0.0292
2451	13	0.58114	19.7637	0.05987	0.0768	0.0243	...	2594	...	13	0.64749	20.4907	0.09116	0.1575	0.0245
2454	13	0.65046	20.2845	0.13473	0.1500	0.0243	0.1590	2602	...	13	0.666981	20.0542	0.07331	0.1476	0.0243
2455	16	0.61853	19.8051	0.13443	0.1407	0.0289	0.1590	2607	...	13	0.59903	19.9719	0.05932	0.1197	0.0243
2457	16	0.65777	19.9817	0.13443	0.1592	0.0292	0.1590	2610	...	13	0.69146	20.2495	0.04707	0.1636	0.0245
2458	16	0.50568	19.9917	0.08380	0.0891	0.0289	0.0597	2616	...	13	0.67396	20.1020	0.06841	0.1510	0.0245
2459	16	0.55545	19.8929	0.04334	0.1195	0.0289	...	2622	...	16	0.70984	19.9135	0.06841	0.1753	0.0292
2461	13	0.66070	20.0663	0.10078	0.1449	0.0243	0.1078	2617	...	16	0.68110	20.3109	0.06647	0.1768	0.0292
2472	13	1.08891	21.0285	0.04027	0.2643	0.0306	...	2620	...	13	1.14380	20.9492	0.07324	0.2439	0.0250
2475	13	0.82174	20.5048	0.10183	0.2188	0.0250	...	2621	...	13	0.97878	20.6458	0.06112	0.2496	0.0250
2478	16	0.52421	19.9429	0.06316	0.1900	0.0289	...	2622	...	13	0.52331	0.05718	0.0722	0.0243	0.0621
2491	16	0.69385	20.2091	0.06395	0.1784	0.0292	...	2623	...	13	0.84819	20.3273	0.06631	0.2146	0.0250
2494	13	0.68420	19.4728	0.11406	0.1301	0.0243	...	2624	...	13	0.89365	20.6794	0.07054	0.2452	0.0250
2495	13	0.52068	19.2362	0.07727	0.1030	0.0243	0.0775	2627	...	13	0.58119	20.1524	0.07086	0.1193	0.0243
2503	13	0.57994	19.6307	0.07727	0.0761	0.0243	0.0775	2631	...	13	1.09759	20.7569	0.03792	0.2434	0.0250
2505	13	0.44194	19.5523	0.06396	0.06115	0.0243	0.0827	2623	...	16	0.98491	20.6245	0.03859	0.2445	0.0287
2506	13	0.44775	20.4853	0.06581	0.0813	0.0243	...	2633	...	16	0.60596	19.7528	0.05176	0.1356	0.0289
2507	13	0.65002	20.5516	0.05708	0.1612	0.0245	0.0829	2639	...	16	0.74011	19.8492	0.05066	0.1829	0.0292
2512	13	0.76623	20.1576	0.09621	0.1840	0.0245	0.1960	2649	...	13	0.50078	19.5811	0.07831	0.0779	0.0243
2513	13	0.58753	20.1112	0.08314	0.1202	0.0243	0.1603	2650	...	13	0.73413	19.3363	0.06955	0.1389	0.0243
2515	13	0.74724	20.5557	0.09173	0.1987	0.0245	0.0250	2657	...	13	0.46187	18.4020	0.12911	0.0486	0.0244
2516	13	0.84587	20.0317	0.07771	0.1974	0.0245	...	2666	...	13	0.39746	18.4351	0.03879	0.0374	0.0244
2517	13	0.643359	20.3556	0.10313	0.1488	0.0243	0.0793 ^{a,b}	2668	...	16	0.46489	19.5665	0.03653	0.0831	0.0289
2522	13	0.66416	20.4527	0.09737	0.1624	0.0245	0.1562	2672	...	13	0.67262	19.6900	0.03718	0.1217	0.0289
2530	13	0.56802	19.7513	0.11501	0.1026	0.0243	...	2695	...	16	0.67403	20.5999	0.05555	0.1731	0.0245
2532	13	0.69960	20.4157	0.08593	0.1742	0.0245	...	2696	...	13	0.64731	19.5626	0.02219	0.1451	0.0289
2535	13	0.66319	19.5869	0.14319	0.1278	0.0243	...	2698	...	16	0.57138	19.4338	0.08982	0.1163	0.0289
2545	13	0.76899	19.8956	0.07205	0.1720	0.0245	...	2706	...	16	0.74385	20.1832	0.04961	0.1783	0.0245
2551	13	0.50094	20.1173	0.07791	0.0903	0.0243	0.1764	2711	...	13	0.1330 ^b
2552	16	0.68599	20.2365	0.05088	0.1764	0.0292	0.1330 ^b

^a The photometric redshift estimate differs significantly from the single-galaxy spectroscopic redshift.^b This spectroscopic redshift was obtained after the photometric redshift estimate and was not used in the derivation.

notably X-ray and radio, we will examine cluster M/L ratios, morphologies, cooling flows, the cluster fundamental plane, and radio properties of elliptical galaxies. Each paper will focus on a specific study of this vast statistical sample. Finally, the entire CCD data set (images as well as catalogs) will be released to the astronomical community.

R. R. G. was supported in part by an NSF fellowship, NASA GSRP NGT5-50215, and a Kingsley fellowship. We

thank the Norris Foundation for their generous support of the DPOSS project. We also thank the Palomar TAC and directors for generous time allocations for the DPOSS calibration effort. Numerous past and present Caltech undergraduates (V. Desai, V. Hradecky, J. Meltzer, B. Stalder, J. Hagan, R. Stob, I. Cotoros, and J. Kollmeier) assisted in taking the data utilized in this paper.

REFERENCES

- Abell, G. O. 1958, *ApJS*, 3, 211
 Abell, G. O., Corwin, H. G., & Olowin, R. P. 1989, *ApJS*, 70, 1
 Binggeli, B. 1982, *A&A*, 107, 338
 Brunner, R. J., Connolly, A. J., Szalay, A. S., & Bershady, M. A. 1997, *ApJ*, 482, L21
 Butcher, H., & Oemler, A., Jr. 1978, *ApJ*, 226, 559
 Connolly, A. J., Csabai, I., Szalay, A. S., Koo, D. C., Kron, R. C., & Munn, J. A. 1995, *AJ*, 110, 2655
 Dalton, G. B., Efstathiou, G., Maddox, S. J., & Sutherland, W. J. 1994, *MNRAS*, 269, 151
 Djorgovski, S. G., Gal, R. R., Odewahn, S. C., de Carvalho, R. R., Brunner, R., Longo, G., & Scaramella, R. 1999, in *Wide Field Surveys in Cosmology*, ed. S. Colombi, Y. Mellier, & B. Raban (Paris: Ed. Frontières), 89
 Dressler, A. 1980, *ApJ*, 236, 351
 Frei, Z., & Gunn, J. E. 1994, *AJ*, 108, 1476
 Fukugita, M., Ichikawa, T., Gunn, J. E., Doi, M., Shimasaku, K., & Schneider, D. P. 1996, *AJ*, 111, 1748
 Gal, R. R., de Carvalho, R. R., Odewahn, S. C., Djorgovski, S. G., & Margoniner, V. E. 2000, *AJ*, 119, 12
 Gunn, J. E., & Weinberg, D. H. 1995, in *Wide Field Spectroscopy and the Distant Universe*, ed. S. Maddox & A. Aragón-Salamanca (Singapore: World Scientific), 3
 Gwyn, S. D. J., & Hartwick, F. D. A. 1996, *ApJ*, 468, L77
 Hogg, D. W., et al. 1998, *AJ*, 115, 1418
 Jarvis, J. F., & Tyson, J. A. 1979, *Proc. SPIE*, 172, 422
 Jefferys, W. H., Fitzpatrick, M. J., & McArthur, B. E. 1987, *Celest. Mech.*, 41, 39
 Margoniner, V. E., & de Carvalho, R. R. 2000, *AJ*, 119, 1562
 Miller, C. J., Batuski, D. J., Slinglend, K. A., & Hill, J. M. 1999, *ApJ*, 523, 492
 Schlegel, D. J., Finkbeiner, D. P., & Davis, M. 1998, *ApJ*, 500, 525
 Struble, M. F., & Rood, H. J. 1991, *ApJS*, 77, 363
 ———. 1999, *ApJS*, 125, 35
 Thuan, T. X., & Gunn, J. E. 1976, *PASP*, 88, 543
 Tody, D. 1986, *Proc. SPIE*, 627, 733
 Valdes, F. 1982, *Proc. SPIE*, 331, 465
 van Haarlem, M. P., Frenk, C. S., & White, S. D. M. 1997, *MNRAS*, 287, 817
 Wade, R. A., Hoessel, J. G., Elias, J. H., & Huchra, J. P. 1979, *PASP*, 91, 35